Published in final edited form as:
Cancer Immunol Res. 2015 January ; 3(1): 68–84. doi:10.1158/2326-6066.CIR-14-0192.

T cells bearing a chimeric antigen receptor against prostate-specific membrane antigen mediate vascular disruption and result in tumor regression

Stephen P. Santoro[1], **Soorin Kim**[1], **Gregory T. Motz**[1], **Dimitrios Alatzoglou**[1], **Chunsheng Li**[1], **Melita Irving**[2], **Daniel J. Powell Jr.**[1], and **George Coukos**[1,2,3]

[1]Ovarian Cancer Research Center, Perelman School of Medicine, University of Pennsylvania, Philadelphia, Pennsylvania, USA [2]Ludwig Center for Cancer Research at the University of Lausanne, Epalinges, Switzerland [3]Department of Oncology, University Hospital of Lausanne (CHUV), Lausanne, Switzerland

Abstract

Aberrant blood vessels enable tumor growth, provide a barrier to immune infiltration, and serve as a source of pro-tumorigenic signals. Targeting tumor blood vessels for destruction, or tumor vascular disruption therapy, can therefore provide significant therapeutic benefit. Here we describe the ability of chimeric antigen receptor (CAR)-bearing T cells to recognize human prostate-specific membrane antigen (hPSMA) on endothelial targets *in vitro* as well as *in vivo*. CAR T cells were generated using the anti-PSMA scFv, J591, and the intracellular signaling domains: CD3ζ, CD28, and/or CD137/4-1BB. We found that all anti-hPSMA CAR T cells recognized and eliminated $PSMA^+$ endothelial targets *in vitro*, regardless of the signaling domain. T cells bearing the 3rd generation anti-hPSMA CAR, P28BBζ, were able to recognize and kill primary human endothelial cells isolated from gynecologic cancers. In addition, the P28BBζ CAR T cells mediated regression of hPSMA-expressing vascular neoplasms in mice. Finally, in murine models of ovarian cancers populated by murine vessels expressing hPSMA, the P28BBζ CAR T cells were able to ablate $PSMA^+$ vessels, cause secondary depletion of tumor cells, and reduce tumor burden. Taken together, these results provide strong rationale for the use of CAR T cells as agents of tumor vascular disruption, specifically those targeting PSMA.

Keywords

Chimeric antigen receptor; Adoptive therapy; Vascular disruption; PSMA; Endothelial cell

Corresponding Author: George Coukos (george.coukos@chuv.ch) Professor and Chair, CHUV Department of Oncology, Director Ludwig Cancer Research Center, University of Lausanne Switzerland. T: +41 (0)21 314 06 27.

Conflict of Interest: None

Introduction

The process of tumor development is intricately linked to changes in the local tumor microenvironment. In addition to tumor cells, the microenvironment comprises immune cells, fibroblasts, and aberrant tumor blood vessels, as well as non-cellular components such as signaling molecules and the extracellular matrix. The relationship of the tumor with the microenvironment is dynamic, and cross talk between the two contributes to cancer progression. Within the microenvironment, tumor blood vessels play a central role in cancer progression, providing both oxygen and nutrient exchange to the tumor (1). In addition, endothelial cells lining the blood vessels (*i.e.*, the endothelium) can provide growth signals, such as interleukin (IL) 6 (2), which promote tumor cell proliferation. Tumor endothelial cells are also able to secrete angiocrine factors that contribute to the stemness of nearby cancer cells, promoting both disease severity and resistance to chemotherapy (3). Finally, the tumor endothelium provides a physical barrier to immune cell infiltration, actively protecting the tumor from immunosurveillance (4, 5). We previously demonstrated that activation of endothelin B receptor on the tumor endothelium initiates mechanisms that inhibit T-cell adhesion and subsequent tumor penetration (4). In addition, we showed that tumor blood vessels up-regulate FasL in response to prostaglandin, vascular endothelial growth factor A (VEGF-A), and IL10. FasL expression by the tumor endothelium preferentially kills $CD8^+$ T cells while leaving T regulatory cells (Treg) unharmed (5). Together these findings emphasize the importance of the tumor vasculature in cancer progression and indicate that the destruction of these vessels may have an important impact on tumor development.

T cells can be engineered to recognize tumor or tumor vascular-specific antigens through transduction with either an exogenous T-cell receptor (TCR) or a chimeric antigen receptor (CAR). CARs are composed of a tumor-targeting moiety, most often an scFv, linked to a transmembrane region and intracellular signaling domains that activate the T cell upon antigen engagement (6). They offer a significant advantage over TCRs in that they are MHC-independent (*i.e.*, a single universal receptor can be used to treat all patients whose tumor or vasculature expresses the target antigen regardless of their MHC haplotype). Several cell-surface targets have been identified to distinguish the tumor endothelium from normal vessels. The VEGF receptors (VEGFRs), for example, are highly expressed on the vasculature of a broad range of solid tumors (7), and CAR T cells directed against these receptors have been shown to destroy the tumor vasculature and impair tumor growth (8,9). Although efficacious against these targets in mouse models, CAR T cells have not yet been developed against additional tumor vascular antigens.

Prostate-specific membrane antigen (PSMA), best known as a prostate cancer-specific target, is a surface glycoprotein abundantly expressed on the endothelium of many solid tumors, but not on the normal vasculature (10–11). PSMA is a 750 amino acid type II membrane-bound protein transcribed from the *PSMA* locus, which encodes a number of splice variants, including multiple membrane-bound and cytosolic isoforms (12,13). Interestingly, the ratio of membrane to cytosolic PSMA dramatically increases in prostate cancer (14). Recent studies have demonstrated that PSMA expression confers a proliferative advantage to tumor cells through its function as a hydrolase of poly- and gamma-glutamated

folate (15). As such, it is presumed that PSMA plays a metabolic role on the activated tumor endothelium. Additional functions have also been ascribed to PSMA. For example, mice lacking PSMA exhibit impaired angiogenesis as a result of defects in endothelial cell invasion (16). The expression of PSMA by the LNCaP prostate cancer cell line has been shown to induce the expression and secretion of IL6, which increases the proliferative potential of tumor cells (17). Since the tumor endothelium has been shown to be an important source of IL6 (2), it is conceivable that PSMA signaling is also involved in the production of IL6 from these cells. Taken together, these data implicate PSMA as a contributor to tumor progression, and provide strong rationale for the generation of CAR T cells against the tumor endothelial cells on which it is expressed.

Here we describe the development of CAR T cell therapy directed against human (h)PSMA expressed by the tumor endothelium and provide proof of principle that this approach may be used to elicit tumor vascular disruption. We demonstrate that anti-hPSMA CAR-bearing T cells function against endothelial targets *in vitro* regardless of the signaling domain incorporated into their design (ζ, 28ζ, BBζ, or 28BBζ). We also establish that the 3rd generation CAR T cells, containing the 28BBζ signaling domain, are able to recognize primary tumor endothelial cells isolated from subjects with gynecologic cancer. Furthermore, we show that *in vivo* the P28BBζ T cells are able to resolve murine hemangioma and hemangiosarcoma tumors, which express hPSMA. Using state of the art luciferase imaging technology we show directly, for the first time, that CAR T cells are able to eliminate endothelial cells within solid tumors and that vessel destruction results in secondary depletion of tumor cells, as well as reduced tumor burden. Overall our work demonstrates that PSMA is a valid target for CAR T cell-mediated tumor blood vessel destruction, and provides insight into the importance of vascular disruption in the broader context of cancer therapeutics.

Materials and Methods

CAR Construction

The J591 (18) and MOv19 (19) scFvs were gifts from M. Sadelain and D. Powell, respectively. The pELNS lentiviral vector and the genes encoding the CAR signaling domains ζ, 28ζ, BBζ, and 28BBζ were gifts from C. June (20). pELNS is a third generation self-inactivating lentiviral expression cassette based on pRRL-SIN-CMV-eGFP-WPRE (21), with transgene expression driven by the EF-1α promoter. The constructs were engineered to express an upstream eGFP reporter separated from the CAR by a T2A sequence. The J591 and MOv19 scFvs were amplified via PCR and subcloned into an intermediary vector (pCLPS) using 5′ BamHI and 3′ NheI restriction enzyme cut sites. 5′ primer, J591F = ATCGggatccGTGCAGCTGCAGCAGTCAGG and 3′ primer, J591R = GCTAgctagcCCGTTTCAGGTCCAGCATGG. BamHI and NheI cut sites are underlined, respectively. The resulting constructs contained the full-length CAR construct, including signaling domain(s). The full-length sequence for each CAR was then isolated from the pCLPS vectors using 5′ AvrII and 3′ SalI restriction enzyme cut sites. Finally, the CAR constructs were ligated into the pELNS vector backbone, which was gel-purified after digestion with XbaI (compatible with AvrII) and SalI restriction enzymes.

Lentiviral production

Lentivirus was generated as previously described (22). Briefly, 2.0×10^6 293T cells were plated in T-150 tissue culture flask 18 h before transfection with transgene (15 μg, pELNS) and packaging plasmids (7 μg pVSV-G, 18 μg pRSV-REV, and 18 μg pMDLg/p.RRE). Supernatants were collected at 24 and 48 h and were then combined and concentrated via ultracentrifugation at 28,000 RPM for 3 h. Virus was re-suspended in 2 mL RPMI (10% FBS, 100 IU mL^{-1} penicillin, and 100 μg mL^{-1} streptomycin sulfate), flash frozen, and stored at –80° until needed.

Human T-cell transduction

T cells were isolated from healthy donors by the Human Immunology Core at the University of Pennsylvania under a protocol approved by the University Institutional Review Board. With minor modifications, T cells were transduced as previously described (22). Briefly, T cells were cultured in RPMI supplemented with 10% FBS, 100 IU mL^{-1} penicillin, and 100 μg mL^{-1} streptomycin sulfate. 20 h prior to transduction, 5.0×10^5 T cells were activated using anti-CD3/anti-CD28 coated beads (Invitrogen, Carlsbad, CA) at a 2:1 bead to T cell ratio in RPMI supplemented with 50 IU mL^{-1} recombinant human IL2 (Peprotech, Rocky Hill, NJ). Activated T cells were spinoculated at 1000 g for 90 min with lentivirus [multiplicity of infection (MOI) of 10] and polybrene (8 μg mL^{-1}; Sigma-Aldrich, St. Louis, MO) in a total volume of 1 mL. 24 h after spinoculation, half the media was removed (0.5 mL) and cells were given 1.5 mL of fresh RPMI with 50 IU mL^{-1} recombinant human IL2. The media was replenished every other day with fresh RPMI and IL2 (50 IU mL^{-1}) so that T-cell density did not exceed ~1.0×10^6 mL^{-1}. The T cells were used between 14–28 d after transduction.

Cell Lines

Low-passage (P16) 293T cells purchased from the American Type Culture Collection (ATCC, Manassas, VA) were used for the production of lentivirus particles. The MS1 (mouse pancreatic islet) endothelial cell line was also purchased from the ATCC. Immortalized H5V (mouse heart endothelial cells) were previously acquired (23). 293T, MS1, and H5V cell lines were grown in RPMI supplemented with 10% FBS, 100 IU mL^{-1} penicillin, and 100 μg mL^{-1} streptomycin sulfate. HMEC-1 cells, an SV40 transformed human microvascular endothelial cell line (24), were obtained from the Centers for Disease Control and Prevention (Atlanta, GA) and grown in MCDB 131 media (Invitrogen, Carlsbad, CA) containing mouse EGF (BD, Franklin Lakes, NJ), hydrocortisone (Sigma-Aldrich, St. Louis, MO), 10% FBS, 100 IU mL^{-1} penicillin, and 100 μg mL^{-1} streptomycin sulfate and 1x GlutaMax (Invitrogen, Carlsbad, CA). All cell lines used were tested by the University of Pennsylvania Cell Center (Philadelphia, PA) and found to be mycoplasma-free. No other authentication assay was performed.

Cell Line transduction

Stable expression of luciferase was accomplished by lentiviral transduction of the MS1, H5V, and HMEC-1 cell lines. 2.5×10^5 endothelial cells were placed in a 6-well plate and virus containing the gene for either firefly luciferase or renilla luciferase was added at an

MOI of 10. Media was changed 24 h after transduction. Cells were sorted for either firefly or renilla luciferase based upon reporter expression of the red fluorescent protein, mCherry, (RFP) or the enhanced green fluorescent protein (eGFP), respectively, using a MOFLO cell sorter (Cytomation). Subsequent splits from the luciferase$^+$ lines were then transduced with human PSMA as described above.

Flow Cytometry

CAR T cells were identified primarily through detection of their eGFP reporter. For surface detection, T cells were stained with an APC-conjugated goat anti-mouse F(ab_2) fragment (Jackson, West Grove, PA; #115-136-072). Bcl-xL expression was detected using a mouse anti-human Bcl-xL Ab (SouthernBiotech, Birmingham, AL; clone 7B2.5) after fixation and permeabilization with an intracellular staining kit (eBioscience, San Diego, CA). PSMA was detected using a humanized J591 mAb (gift from N. Bander) and an APC-conjugated anti-human secondary Ab (Jackson, West Grove, PA; #109-136-098). Positive staining was assessed by comparison with a human IgG isotype control Ab (Enzo, Farmingdale, NY; #ALX-804-133-C100). In addition to the J591 mAb, human tumor digests were stained with APC-Cy7-conjugated anti-human CD45 (BD, Franklin Lakes, NJ; clone 2D1), Pacific-Blue-conjugated anti-human CD31 (BioLegend, San Diego, CA; clone WM59), and PE-conjugated anti-folate receptor (R&D, Minneapolis, MN; clone 548908) Abs prior to analysis. Harvested mouse tumors were also stained with the J591 mAb, as well as APC-Cy7-conjugated anti-human CD45 (BD, Franklin Lakes, NJ; clone 2D1) and Pacific-Blue-conjugated anti-mouse CD31 (BioLegend, San Diego, CA; clone 390) Abs. All samples were stained with the fixable viability dye eFlour 506 prior to analysis (eBioscience, San Diego, CA).

T cell proliferation studies

Prior to co-culture with target cell lines, T cells were labeled with CellVue® Claret as described in the kit's technical bulletin (Sigma-Aldrich, St. Louis, MO). Labeling was confirmed by flow cytometry prior to co-culture. 1.0×10^5 CAR T cells were then cultured with 5.0×10^4 HMEC-1 or HMEC-1^{PSMA} at an effector to target (E:T) ratio of 2:1 for 5 days in 48-well flat-bottom plates. Flow cytometry was used to analyze the intensity of CellVue® staining after co-culture. CAR$^+$ T cells were identified by eGFP expression. To quantify the membrane staining between the T cells cultured with the HMEC-1 versus HMEC-1^{PSMA}, the geometric mean fluorescence intensity (MFI) of Cellvue® Claret staining was measured for the CAR-positive T cells. To normalize across multiple donors, the MFI of CellVue® staining on CAR$^+$ T cells after co-culture with HMEC-1^{PSMA} was divided by the MFI of the CAR$^+$ T cells after co-culture with the HMEC-1.

Cytokine Release Assays

IFNγ ELISAs were performed as directed in the Human IFNγ ELISA MAX technical manual (BioLegend, San Diego, CA). For cell line assays, 7.5×10^4 CAR T cells were cultured overnight with 2.5×10^4 endothelial targets (E:T = 3:1). Triplicate cultures were performed in 96-well flat-bottom plates. Supernatants were collected from each well after 18 h. For assays utilizing primary human tumor samples, 9.0×10^4 CAR T cells were cultured

overnight with 3.0×10^4 enriched endothelial targets (E:T = 3:1). Cultures were performed in 96-well flat-bottom plates and supernatants were collected after 18 h.

Cytotoxicity Assays

^{51}Cr release assays were performed as previously described (22). CAR T cells were cultured for 18 h with endothelial targets at E:T ratios of 10:1, 3:1, and 1:1. Specific lysis was calculated as (experimental – spontaneous lysis/maximal – spontaneous lysis) × 100. Luciferase based assays were performed similarly; CAR T cells were co-cultured for 18 h with endothelial targets engineered to express either firefly or renilla luciferase at the ratios indicated in the figure legend(s). Co-cultures were performed in triplicate using opaque 96-well flat-bottom plates in phenol-free RPMI. Single luciferase assay (firefly) measurements were taken according to Luc-Screen® technical manual (Life Technologies, Grand Island, NY), whereas dual luciferase assay (firefly and renilla) measurements were made as directed by the Dual-Glo® technical manual (Promega, Madison, WI). The percentage of specific lysis was calculated as 100 – (luciferase signal treated/luciferase signal untreated × 100). For the bystander killing assays, the number of CAR T cells, as well as the number of antigen negative target cells, remained constant for all ratios (5.0×10^4). PSMA positive targets were added at the ratios described in the figure legend(s).

Time-lapse microscopy

24-well flat-bottom plates were coated with a thin layer (300 μL per well) of Matrigel (BD, Franklin Lakes, NJ) and allowed to solidify at 37° C for 30 min. Next, either 1.0×10^5 HMEC-1 or 1.0×10^5 HMEC-1^{PSMA} endothelial cells were seeded into the wells. Microvessels were given 8 h to form prior to addition of the CAR T cells. After 8 h, 3.0×10^5 CAR T cells were added to each well and images were taken at 0, 24, and 48 h after initiation of the co-culture (E:T = 3:1). Cells were kept in an environmentally controlled chamber at 37° C with 5% CO_2 throughout the experiment. X-Y coordinates were saved for each well so that the identical field of view could be captured at each time point. Pictures were taken using a fluorescence microscope (ECLIPSE Ti; Nikon Corporation, Tokyo, Japan) equipped with a charge-coupled device camera (Photometrics CoolSnap HQ2; Roper Industries, Inc, Sarasota, FL, USA) and NIS-Elements AR software (v 3.2; Nikon Corporation).

Immunohistochemistry

For human tissue microarray (TMA) staining, paraffin-embedded tissues were baked at 60 °C for 1 h, deparrafinized in xylenes, rehydrated in sequential gradations of alcohol, and washed in water. Depending on the Ab, antigen retrieval was performed using either citrate or EDTA buffer. Endogenous peroxidase was inactivated with Dual Endogenous Enzyme block (Dako, Carpnteria, CA). Following Ab staining, TMAs were visualized with diaminobenzidine tetrahydrochloride (Dako, Carpnteria, CA) or an alkaline phosphatase red substrate kit (dual stains). Sections were then counterstained with hematoxylin. Sections were stained with an anti-human PSMA Ab (Dako, Carpnteria, CA; clone 3E6) alone, or in combination with anti-human CD34 Ab (Thermo Scientific, Waltham, MA; rabbit polyclonal). The TMAs were then scanned and analyzed using ImageScope software. For TMAs that included multiple cores from the same subject, individuals were considered

PSMA$^+$ if staining could be confirmed on any of the cores from that subject. Damaged or absent cores were excluded from analysis.

Enrichment of human CD31$^+$ endothelial cells

Human tumor specimens were gathered with approval from the University of Pennsylvania institutional review board in compliance with the US Health Insurance Portability and Accountability Act (HIPAA). Briefly, tumors were mechanically or enzymatically digested to yield single-cell suspensions that were subsequently frozen and stored at –150° C until needed. Samples were rapidly thawed in a 37° C water bath. Viable cells were counted using Trypan Blue. Tumor digests were first depleted for CD45 using Miltenyi anti-human CD45 beads, as per manufacturer's instructions (Miltenyi, San Diego, CA). The CD45$^-$ fraction was then enriched for human CD31 endothelial cells using Miltenyi anti-human CD31 beads (Miltenyi, San Diego, CA). Both the CD45$^-$CD31$^-$ and CD45$^-$CD31$^+$ population were retrieved and analyzed by flow cytometry and/or used in functional assays.

Mice

All protocols were reviewed and approved by the Institutional Animal Care and Use Committee at the University of Pennsylvania. All experiments were done using female NOD.Cg-*Prkdc*^{scid} *Il2rg*^{tm1Wjl}/SzJ (NSG) mice (aged 8–10 weeks) purchased from and housed at the Stem Cell Xenograft Core (SCXC), a germ-free facility at University of Pennsylvania.

In vivo assays with HMEC-1 cells

Matrigel plugs containing HMEC-1 (left flank) and HMEC- 1^{PSMA} (right flank) endothelial cells were injected s.c. into the flanks of mice. CAR-positive T cells were administered via tail vein injection immediately following implantation of the plugs. The number of cells inoculated/injected is noted in the figure legend(s). Mice were sacrificed after 11 days and the Matrigel plugs retrieved and digested with 3U mL^{-1} dispase (Sigma-Aldrich, St. Louis, MO) and 25 μg mL^{-1} DNase to yield single-cell suspensions. The cells collected from the plugs, as well as splenocytes collected from the sacrificed animals, were then stained and analyzed by flow cytometry.

In vivo assays with MS-1 cells

Mice were injected s.c. on each flank with MS1 (left flank) and MS1^{PSMA} (right flank) endothelial cells and CAR-bearing T cells were administered as noted in the figure legend(s). Hemangioma development and response to treatment was monitored twice a week by measuring luciferase luminescence. Mice were injected intraperitoneally with 100 μL of D-Luciferin stock solution (30 mg mL^{-1}, GoldBio, St. Louis, MO), anesthetized using isofluorane, and imaged 20 min after luciferin injection. To avoid bias, the PSMA$^+$ tumor (right flank) was measured first. Mice were then flipped, and the antigen-negative tumor (left flank) was analyzed, typically 1–2 minutes after the right flank. Data were gathered using a Xenogen IVIS imaging system, and analyzed using Living Image software (PerkinElmer, Waltham, MA). When palpable, tumors were measured with Vernier calipers and volumes were calculated using the equation $V=\frac{1}{2}(L \times W^2)$.

In vivo assays with H5V cells

Mice were injected i.v. with $H5V^{PSMA}$ endothelial cells and CAR T cells were administered as noted in the figure legend(s). Tumor development and response to treatment was monitored twice a week by measuring luciferase luminescence. Mice were injected with luciferin as described above, and 20 min after injection the ventral surface of the animals was imaged. Mice were weighed twice per week and sacrificed if/when they lost more than 10% of their initial body mass.

In vivo assays with MS1/ID8 cells

Mice were injected s.c. on each flank with MS1/ID8 (left flank) and $MS1^{PSMA}$/ID8 (right flank) cells and CAR T cells were administered as noted in the figure legend(s). Luciferase luminescence and tumor volume were measured as described for the MS1 tumors. After termination of the $MS1/ID8^{VEGF}$ experiment, the remaining tumors were excised and split for analysis. Half of each tumor was embedded and frozen in Tissue-Tek® optimum cutting temperature medium (VWR, Philadelphia, PA), while the other half was digested overnight in serum-free RPMI containing collagenase (175 collagen digestion units mL^{-1}) and DNAse (20 Kunitz units mL^{-1}). After digestion, tumors were filtered through a 70 μm mesh filter and treated with Ammonium-Chloride-Potassium buffer to lyse red blood cells. Digests were then analyzed by flow cytometry. Tumors not large enough to be split were embedded in O.C.T. and frozen. For the $ID8^{VEGF}$, $MS1/ID8^{VEGF}$, $MS1^{PSMA}/ID8^{VEGF}$ control mice (Fig. 5), eGFP radiance was also measured. The $ID8^{VEGF}$ tumor cells brightly express an eGFP reporter (data not shown). Spectral unmixing for eGFP was performed using the Living Image software, and the results were plotted against luciferase luminescence values taken concurrently (Fig. 5F–J).

Statistical Analysis

Values are expressed as the mean ± either SD or SEM, as indicated in the figure legends. Statistical differences were determined to be significant *at* $P < 0.05$. Specific tests used are described in the figure legends. All analyses were performed using Graphpad Prism Software.

Results

Design and characterization of an anti-vascular CAR targeting endothelial PSMA

The effector function and persistence of CAR-bearing T cells is dependent upon the signaling domains incorporated in their design. Costimulation through CD28 and/or 4-1BB augments CAR T-cell function *in vivo*, generating a more potent antitumor response (18,20). *In vitro*, the impact of costimulation is less clear with studies reporting either no difference in the cytolytic potential of the different generation CAR T cells (20) or enhanced killing using the 2^{nd} and 3^{rd} generation CAR T cells (18). These data suggest that the intrinsic properties of the targeted cell line(s) may influence the functionality of the various CAR T cells, and that costimulation may confer a greater advantage against certain cell types or cell lines. Since the effect of costimulation on CAR T-cell function has not been ascertained for

endothelial targets, we designed a series of CAR constructs containing the ζ, 28ζ, BBζ, or 28BBζ signaling domains and compared their functionality against endothelial cells *in vitro*.

Research from the laboratory of Michel Sadelain has shown that CAR T cells targeted against hPSMA (hereafter referred to as PSMA) are able to eliminate prostate cancer cells *in vitro* as well as *in vivo* (18). The scFv utilized in these constructs was derived from the mouse monoclonal (m)Ab J591, which was also used to identify PSMA on blood vessels within a number of solid tumors (10,11,25). We therefore utilized the J591 scFv in the design of our CAR constructs, which we referred to as Pζ, P28ζ, PBBζ, and P28BBζ, based upon the intracellular signaling domain incorporated into their design. In addition, we also utilized a specificity control CAR, FR28BBζ, which recognizes the non-vascular antigen, human folate receptor alpha (FRα) (19). Each CAR was subcloned downstream of an eGFP reporter within the pELNS lentiviral cassette (Fig. 1A,B). Typical transduction efficiencies ranged from 50–90% in primary human T cells (Fig. 1C). To confirm CAR surface expression, the P28BBζ T cells were stained with a goat anti-mouse $F(ab)_2$ fragment. eGFP expression and CAR surface detection were strongly correlated, validating the use of the eGFP reporter as a proxy for CAR expression (Supplementary Fig. S1).

Although PSMA has been detected on the tumor endothelium *in vivo*, it has not been described on endothelial cells in culture. To ascertain whether cultured human endothelial cells express PSMA, we stained both the immortalized HMEC-1 cell line (24) as well as primary human umbilical vein endothelial cells (HUVEC), using the J591 mAb. We were unable to detect PSMA on either the HMEC-1 (Fig. 1D) or the HUVEC (not shown). We therefore engineered the HMEC-1 cells to express PSMA using lentivirus (Fig. 1D). To compare the ability of each CAR construct to redirect T cells towards endothelial PSMA, we first measured the proliferative capacity of the CAR-bearing T cells in response to the HMEC-1^{PSMA} cell line. All anti-PSMA CAR T cells proliferated in response to the HMEC-1^{PSMA} regardless of their signaling domain (Fig. 1E,F), but did not proliferate in response to the antigen negative HMEC-1 (not shown). There were no statistical differences between the groups. In contrast to the anti-PSMA T cells, control FR28BBζ CAR T cells did not show any significant proliferation in response to the HMEC-1^{PSMA} when compared to untransduced (UNTR) T cells (Fig. 1F). Similarly, we observed that all the anti-PSMA CAR T cells were able to specifically kill the HMEC-1^{PSMA} during overnight co-culture, with no statistically significant differences detected between the anti-PSMA T cells (Fig. 1G). Finally, we compared the ability of each CAR to confer resistance to apoptosis by measuring the anti-apoptotic factor, Bcl-xL, following activation. After co-culture with the HMEC-1^{PSMA}, the P28BBζ T cells induced the highest levels of Bcl-xL expression, although this observation did not reach statistical significance (Supplementary Fig. S2A,B). These data demonstrate that, *in vitro*, all CAR constructs are able to react against endothelial targets regardless of their intracellular signaling domain. Since we found no advantage to using any of the examined signaling domains *in vitro*, and since the third generation CAR T cells (28BBζ) were found to be equivalent or superior to either the 1^{st} (ζ) or 2^{nd} (28ζ or BBζ) generation CAR T cells in the context of tumor control *in vivo* (18), we selected the P28BBζ T cells for further experimentation.

PSMA is expressed on the vasculature of primary and metastatic cancer

PSMA has been detected on tumor blood vessels in a variety of cancers, including ovarian (26) (summarized in Supplementary Fig S3a). To confirm this observation for individuals with ovarian cancer, we performed immunohistochemistry on a TMA composed of 13 primary ovarian cancer specimens and 15 matched metastases (Fig. 2A**,** top row). We observed PSMA expression on vessel-like structures within the majority of tumors, with 12/13 (85%) of the subjects expressing PSMA within their primary ovarian lesion(s), and 14/15 (93%) expressing PSMA on one or more of their metastases (Fig. 2B). We did not identify PSMA on any of the 16 normal ovary cores analyzed. Endothelial expression of PSMA was confirmed by co-staining of the TMA using a CD34 antibody, in addition to the anti-PSMA antibody (Fig. 2A, bottom row). Here we noticed the presence of $CD34^{+}PSMA^{-}$ vessels in some of the cores analyzed (Fig. 2C), corroborating the observations made in other cancers that PSMA expression was heterogeneous on vessels within the tumor (Supplementary Fig. S3B). To define the percentage of endothelial cells expressing PSMA within the tumor, we examined freshly dissociated cancer samples by flow cytometry. In support of our observations by IHC, we found PSMA expression on approximately 40–60% of the $CD45^{-}CD31^{+}$ endothelial cells (Fig. 2D).

Next we asked whether the P28BBζ CAR T cells were capable of recognizing and killing tumor endothelial cells isolated from individuals with cancer. Tumor endothelial cells were enriched from freshly dissociated tumor samples first by negative selection of $CD45^{+}$ leukocytes and then by positive selection of $CD31^{+}$ endothelial cells using magnetic bead sorting. CD31-enriched and CD31-depleted tumor-derived cells were then incubated with P28BBζ CAR T cells for 18 h. We found that P28BBζ CAR T cells substantially reduced the percentage of $PSMA^{+}$ endothelial ($CD45^{-}CD31^{+}$) cells in primary tumor-derived cells. The control FR28BBζ CAR T cells had no impact on the percentage of $PSMA^{+}$ cells remaining in the culture (Fig. 2E). To confirm the activation of the P28BBζ CAR T cells in these cultures, we performed IFNγ ELISA on the supernatants collected from the overnight co-cultures of the P28BBζ CAR T cells with either the CD31-enriched or the CD31-depleted populations. IFNγ was produced in all instances in which the P28BBζ T cells were co-cultured with the CD31-enriched endothelial cells (Fig. 2F). Interestingly, we also observed IFNγ production in one of the CD31-depleted co-cultures (Fig. 2F, #1913). To determine whether expression of PSMA by the tumor cells could explain this observation, we stained the $CD45^{-}CD31^{-}$ population for PSMA as well as FRα, a tumor-specific antigen in ovarian cancer (27). For subject #1913, we found that a substantial portion of the $FR\alpha^{+}$ cells stained positive for PSMA (Supplementary Fig. S3C). Because the main cell populations in the $CD45^{-}CD31^{-}$ fraction are tumor cells and stroma fibroblasts, and because the stroma of gynecologic cancers does not express the FRα (28,29), these findings suggest that tumor cells in some individuals with ovarian cancer may also express PSMA, which has been noted for other cancers (30). Collectively, our data along with those in numerous published reports (Supplementary Fig. S3A) demonstrate that PSMA is expressed widely on the tumor vasculature and provide rationale for the development of CAR T-cell therapy against this antigen.

P28BBζ CAR T cells target human tumor vasculature expressing PSMA

To simulate the interactions of P28BBζ CAR T cells with human tumor blood vessels *in vitro*, we plated HMEC-1 or HMEC-1^{PSMA} endothelial cells on Matrigel basement membranes and allowed the cells to self-assemble into microvessels (8 h). Upon assembly, T cells were added, and the cultures were monitored for 48 h by fluorescence microscopy (Fig. 3A). As early as 24 h after addition of the T cells to the microvessels, we observed specific localization of the P28BBζ CAR T cells with the HMEC-1^{PSMA} microvessels, and within 48 h the HMEC-1^{PSMA} vessels were destroyed (Fig. 3B). In contrast, the antigen-negative microvessels persisted throughout the duration of the co-culture with the P28BBζ CAR T cells. As expected, the T cells directed against FRα did not impact the persistence of either the HMEC-1 or HMEC-1^{PSMA} microvessels (Fig. 3A). These data indicate that the P28BBζ CAR T cells were able to specifically recognize PSMA^{+} vessels, but not normal (PSMA^{-}) vascular structures *in vitro*.

We next assessed the ability of the P28BBζ CAR T cells to recognize human endothelial cells expressing PSMA *in vivo*. We transplanted Matrigel plugs containing either HMEC-1 (left flank) or HMEC-1^{PSMA} (right flank) cells into severely immunodeficient NSG mice (Fig. 3C). Immediately after transplantation of the Matrigel plugs, mice were given an intravenous (i.v.) injection of either P28BBζ CAR T cells or control FR28BBζ CAR T cells. The plugs and spleens were harvested 11 days after inoculation and analyzed for the presence of CAR-positive T cells via flow cytometry. In mice receiving the P28BBζ T cells, we found large numbers of CAR T cells in the plugs harboring the HMEC-1^{PSMA} cells, whereas the plugs containing control HMEC-1 cells were largely devoid of T cells (Fig. 3D,E). Similarly, very few FR28BBζ control T cells were found in the plugs containing either the PSMA positive or negative endothelial cell lines. Finally, we measured the percentage of CAR T cells found in the spleens of the treated mice and found significantly more P28BBζ CAR T cells when compared to mice that received the FR28BBζ control T cells (Fig. 3E). Together, these data demonstrate that the P28BBζ CAR T cells are able to recognize and accumulate on PSMA^{+} endothelial cells and that they are able to persist *in vivo* in the presence of the antigen.

P28BBζ CAR T cells eliminate PSMA^{+} vascular neoplasms

Because the HMEC-1 model did not reproducibly form vascular structures *in vivo*, we used two well-established murine endothelial models, the MS1 murine hemangioma model (31) and the H5V hemangiosarcoma model (23), to test the therapeutic efficacy of the P28BBζ CAR T cells. First, we engineered the expression of human PSMA onto the surface of the MS1 and H5V endothelial cell lines (Fig. 4A). To assess the specificity and ability of the P28BBζ T cells to react against these endothelial targets, we performed an IFNγ ELISA on supernatants collected from overnight co-cultures of the P28BBζ T cells with the PSMA-negative endothelial cell lines (MS1 and H5V) and their PSMA-transduced counterparts (MS1^{PSMA} and H5V^{PSMA}). We found that IFNγ production was limited to the cultures containing the P28BBζ CAR T cells and PSMA^{+} endothelial cells (Fig. 4B). Next, we asked whether the P28BBζ CAR T cells would be able to specifically kill the PSMA^{+} endothelial cells. Using a chromium release assay, we found that the P28BBζ CAR T cells killed the

majority of the $PSMA^+$ endothelial cells within 18 h of co-culture, while the $PSMA^-$ cell lines were spared (Fig. 4C).

Next, we injected NSG mice subcutaneously (s.c.) with MS1 cells (left flank) and $MS1^{PSMA}$ cells (right flank), both of which had been previously engineered to express firefly luciferase to allow us to make non-invasive, real time tumor measurements throughout tumor progression and treatment. The hemangioma lesions were allowed to develop and tumor growth was monitored via luciferase luminescence. Mice were treated with a single i.v. administration of 5.0×10^6 CAR T cells 24 days after tumor inoculation (Fig. 4D). In mice receiving the P28BBζ CAR T cells, we observed rapid regression of the $MS1^{PSMA}$ hemangiomas, whereas the antigen-negative MS1 flank was unaffected (Fig. 4E). Macroscopic examination of the hemangiomas upon sacrifice revealed that injection of the P28BBζ CAR T cells led to complete regression of the $PSMA^+$ tumors (Fig. 4F). In contrast, the control FR28BBζ CAR T cells had no impact on either of the hemangiomas. We also tested the P28BBζ T cells against larger, more developed, MS1 and $MS1^{PSMA}$ hemangiomas (Supplementary Fig. S4A). Again, we observed rapid regression of the $MS1^{PSMA}$ tumors after administration of the P28BBζ CAR T cells, as measured by both luciferase luminescence and caliper measurement (Supplementary Fig. S4B), which we confirmed visually upon sacrifice of the mice (Supplementary Fig. S4C). Importantly, in both treatment models the P28BBζ CAR T cells demonstrated specificity and reactivity exclusively against the $PSMA^+$ tumors.

Finally, we assessed the ability of the P28BBζ CAR T cells to treat murine H5V hemangiosarcoma, an aggressive vascular target that metastasizes to the lung. Twenty-one days following i.v. inoculation with $H5V^{PSMA}$ endothelial cells, NSG mice were given three i.v. injections of 5.0×10^6 CAR T cells 72 h apart (Fig. 4G). We monitored the progression and response of the tumors to treatment by luciferase luminescence, and mice were sacrificed upon losing 10% of their initial body mass. By the third injection of CAR T cells, the $H5V^{PSMA}$ cells were nearly undetectable in the P28BBζ CAR treatment group, whereas no effect was seen in the FR28BBζ CAR treatment group (Fig. 4H,I). Furthermore, mice treated with the P28BBζ CAR T cells lived significantly longer than those treated with PBS or FR28BBζ T cells (Fig. 4J). Collectively, results from these models demonstrate that the P28BBζ CAR T cells are able to traffic to and eliminate aberrant $PSMA^+$ tumor vessels *in vivo*, and that PSMA-targeting CAR T cells are potent mediators of tumor vascular disruption.

CAR T cells ablate $PSMA^+$ vasculature in solid tumors

Elimination of tumor vessels by vascular disrupting agents can cause regression of solid tumors (32). To test whether the P28BBζ CAR T cells could also elicit this effect, we employed a pair of syngeneic vasculature/tumor chimeric transplant models. MS1 endothelial cells have been co-injected with both murine (ID8) and human (2008) tumor cells, and were found to form functional vessels within both models, as assessed by immunohistochemistry and hemoglobin content (33–35). We therefore interrogated the impact of P28BBζ-mediated vessel destruction in the MS1/ID8 tumor model, as well as in the $MS1/ID8^{VEGF}$ tumor model, in which the ID8 tumor cells were engineered to

overexpress mouse $VEGF_{164}$ (36). The endothelial and tumor cells were combined at an optimal ratio, such that the majority of tumor blood vessels would be derived from the MS1/$MS1^{PSMA}$ endothelial cells. Fig. 5A illustrates a representative experiment where mice were inoculated with $ID8^{VEGF}$, MS1/$ID8^{VEGF}$, or $MS1^{PSMA}$/$ID8^{VEGF}$ tumors. By day 41, the majority of the $CD31^+$ endothelial cells from the $ID8^{VEGF}$/$MS1^{PSMA}$ tumors were found to express PSMA by immunofluorescence microscopy and exhibit typical vessel morphology, confirming that the exogenous MS1 endothelial cells were substantially contributing to the tumor vasculature in this model (Fig. 5B). These results were verified by flow cytometry, which showed that more than 65% of $CD31^+$ endothelial cells purified from the tumors were $PSMA^+$ (Fig. 5C). Importantly, the $CD31^+$ endothelial cells contributed less than 2% to the total cells isolated from the chimeric tumors, which was similar to what was observed for the $ID8^{VEGF}$-only tumors, in which the vasculature was derived from endogenous endothelial cells. Therefore, we concluded that the majority of the tumor was derived from the $ID8^{VEGF}$ cells or stromal cells and not the co-injected MS1 endothelial cells (Fig. 5D). In addition, we noted no difference in the tumor growth kinetic between the $ID8^{VEGF}$ alone tumors or the $ID8^{VEGF}$ tumors augmented with MS1 or $MS1^{PSMA}$ cells (Fig. 5E), further demonstrating that the chimeric tumors reproduced a “normal” tumor growth condition, and confirming that the addition of MS1 or $MS1^{PSMA}$ cells did not substantially contribute to the volume of these tumors.

We next asked whether the proportion of MS1-derived vessels was consistent throughout tumor development. For these experiments we used MS1 and $MS1^{PSMA}$ cells engineered to express firefly luciferase and $ID8^{VEGF}$ tumor cells engineered to express eGFP. In mice injected with either MS1/$ID8^{VEGF}$ or $MS1^{PSMA}$/$ID8^{VEGF}$ tumors, we compared seven longitudinal luciferase luminescence measurements, obtained between days 17 and 41, to seven longitudinal eGFP radiant efficiency measurements obtained at the same time points (Fig. 5F–J). We performed linear regression analyses on the values obtained and found that endothelial luminescence was strongly correlated with tumor radiant efficiency (Fig. 5F–J), indicating that the exogenous endothelial cells expanded proportionally to the tumor cells. Thus, we concluded that within this tumor model the exogenous endothelial cells provide the main source of tumor endothelial cells required for neovascular formation and that the contribution of MS1 endothelial cells was consistent throughout tumor development, beginning as early as 17 days after tumor inoculation. Overall, our data indicate that the presence of the MS1 or $MS1^{PSMA}$ vessels largely obviates the need for endogenous endothelial cell recruitment, and that the MS1 endothelial cells do not constitute a significant portion of the cells within the tumor, supporting the assertion that the MS1 cells are predominantly forming tumor blood vessels and not contributing substantially to the overall tumor mass. Finally, we have demonstrated that the MS1 and $MS1^{PSMA}$ endothelial cells can be followed non-invasively during tumor growth within this model, allowing for their persistence or elimination to be monitored after treatment with CAR T cells.

To test the ability of P28BBζ CAR T cells to ablate tumor vasculature *in vivo*, we first utilized the MS1/ID8 tumor model. NSG mice were injected with MS1/ID8 (left flank) and $MS1^{PSMA}$/ID8 (right flank) tumors, which were allowed to develop for 81 days before treatment with a single injection of 1.0×10^7 CAR T cells (Supplementary Fig. 5A). We

found that the P28BBζ CAR T cells were able to eliminate the MS1^{PSMA} endothelial cells quickly, as indicated by luciferase luminescence measurements (Supplementary Fig. 5B, lower panel). In contrast, vessels within the MS1/ID8 tumors were unaffected by the P28BBζ CAR T cells (Supplementary Fig. 5B, upper panel). Administration of the FR28BBζ CAR T cells had no impact on the tumor blood vessels, confirming the specificity of the P28BBζ T cells.

Since VEGF plays an important role in the development and stabilization of new tumor vessels, and has been implicated in tumor resistance to pharmacologic vascular disruption agents (VDAs) (37), we next sought to evaluate the *in vivo* impact of the P28BBζ CAR T cells on the vasculature of solid tumors expressing high levels of VEGF-A using the ID8^{VEGF} model (36). The MS1/ID8^{VEGF} tumors grew more rapidly than the MS1/ID8 tumors, necessitating that those mice be sacrificed within approximately 40 days to avoid ulceration. Mice were therefore treated earlier and with three injections of 5.0×10^6 CAR T cells, beginning 25 days after tumor inoculation (Fig. 6A). P28BBζ CAR T cells induced rapid regression of the PSMA$^+$ MS1 endothelial cells but had no effect on the control MS1 cells (Fig. 6B). In addition, the control FR28BBζ CAR T cells had no impact on the blood vessels of either tumor. Upon sacrifice we collected and enzymatically dissociated all tumors, which were subsequently stained using antibodies for CD31 and PSMA and analyzed via flow cytometry. No CD31$^+$PSMA$^+$ endothelial cells were found within the tumors of the P28BBζ-treated mice. In control treated mice, between 60–80% of the CD31$^+$ endothelial cells were PSMA$^+$ within the MS1^{PSMA}/ID8^{VEGF} tumors (Fig. 6C). Following successful treatment, CD31$^+$ endothelial cells accounted for less than 0.5% of the total live cells isolated from the tumors, which was lower than either the untreated tumors or tumors treated with control FR28BBζ CAR T cells (Fig. 6D). These findings indicate that, similar to VDAs, CAR T cells can trigger regression of established tumor vasculature.

CAR T cells induce secondary loss of tumor cells and regression of solid tumors

To assess whether vascular disruption was causing secondary loss of tumor cells, we examined the effects of P28BBζ CAR T cells on tumor growth in the experiments described above. In the MS1/ID8 model (outlined in Supplementary Fig. 5A), treatment with P28BBζ CAR T cells led to a significant decrease in the overall size of the MS1^{PSMA}/ID8 tumors, but not of the antigen-negative MS1/ID8 tumors (Supplementary Fig. 5C). In addition, growth of MS1^{PSMA}/ID8^{VEGF} tumors was significantly impaired in P28BBζ-treated mice (Supplementary Fig. 6A,B). This response was dose-sensitive, as mice treated with a single injection of 1×10^7 CAR T cells did not eliminate PSMA$^+$ endothelial cells as rapidly and did not inhibit the growth of ID8^{VEGF} tumors as effectively as mice treated with three injections of 5×10^7 CAR T cells. These data demonstrate that even in the context of VEGF overexpression, elimination of the antigen-positive vasculature by CAR T cells can lead to significant tumor regression.

Given that endothelial cells account for less than 2% of the cells found within the MS1/ID8^{VEGF} and MS1^{PSMA}/ID8^{VEGF} tumors (see Fig. 5D), we hypothesized that the regression observed in the P28BBζ-treated mice was not merely reflecting the loss of MS1^{PSMA} cells from the ID8^{VEGF} tumors, but rather indicating a significant loss of tumor cells in response

to T cell-mediated vascular disruption. To ascertain whether this was true, we developed an $ID8^{VEGF}$ model in which the tumor cells expressed firefly luciferase and the MS1 cells did not. As before, NSG mice were inoculated with MS1/$ID8^{VEGF}$ (left flank) and $MS1^{PSMA}$/$ID8^{VEGF}$ (right flank) tumors. Three administrations of 5.0×10^7 CAR T cells were given, beginning on day 22 (Fig. 7A). Both luciferase luminescence and tumor volume measurements revealed that treatment with P28BBζ T cells impaired tumor growth (Fig. 7B). To determine if the P28BBζ T cells were mediating tumor cell destruction, we compared the fold-change in tumor cell luminescence from mice receiving the P28BBζ T cells. We observed a significant decrease in tumor luminescence from the $MS1^{PSMA}$/$ID8^{VEGF}$ tumors after the second injection of P28BBζ T cells, between days 24 and 28 (Fig. 7C). In contrast, we observed a significant increase in signal from the antigen negative MS1/$ID8^{VEGF}$ tumors during that same period (Fig. 7C). Upon sacrifice of the animals, we confirmed elimination of the $MS1^{PSMA}$ endothelial cells via flow cytometry (data not shown). Together, these data demonstrate that destruction of the vasculature does indeed result in tumor cell loss.

Finally, we sought to determine whether bystander killing of adjacent $ID8^{VEGF}$ tumor cells could explain the reduction in tumor signal we observed in this model. We performed an *in vitro* killing assay in which we co-cultured $MS1^{PSMA}$ endothelial cells overnight at increasing ratios with $ID8^{VEGF}$ tumor cells and T cells. $MS1^{PSMA}$ cells were eliminated by the P28BBζ CAR T cells, but the $ID8^{VEGF}$ cells were unaffected by these T cells (Fig. 7D). These data suggest that tumor regression *in vivo* occurred through indirect loss of tumor cells, related to the disruption of the vasculature, rather than a direct bystander effect.

Discussion

Recent clinical trials have demonstrated the efficacy of CAR T cell-based immunotherapy for individuals with advanced cancer. Remarkable responses have been reported, for example, in patients receiving CD19-specific CAR T-cell therapy for the treatment of acute lymphocytic leukemia (38–40). In addition, active remission has been reported in patients with neuroblastoma after treatment with CAR T cells directed against the ganglioside, GD2 (41). A critical component to the clinical success of these adoptive CAR T-cell therapies is the choice of target antigen. Ideally the antigen should be immunogenic, related to oncogenesis, and selectively expressed on the tumor tissue. One such tumor vascular marker is PSMA whose widespread distribution on vessels of many cancers makes it an ideal target for T cell-mediated vascular disruption. Here we have shown that T cells bearing a CAR against PSMA can destroy the tumor vasculature and elicit tumor regression. Importantly, our data also demonstrate that T cells can act as potent mediators of vascular disruption, thereby justifying the continued pursuit of this therapeutic approach.

One major advantage of using CAR T cells to disrupt the tumor vasculature, as opposed to conventional VDAs, is their ability to self-replicate and to persist long-term in patients (38). In addition, CAR T cells can trigger epitope spreading and help to reprogram the tumor microenvironment (42). Given the persistence and efficacy of CAR T cells, a second critical component to the clinical success of CAR T-cell therapy is safety. This cannot be overstated, as unexpected CAR cross-reactivity with healthy tissues has, unfortunately,

resulted in patient deaths (43). Prior to this study, tumor blood vessels destruction had been demonstrated successfully using CAR T cells engineered to recognize VEGFR-1 and VEGFR-2 (11) or VEGFR-2 alone (10). Although encouraging, VEGF receptors are also expressed by normal endothelial cells throughout the body and thus represent a significant risk for "on-target/off-tumor" toxicity. In contrast, PSMA has not been found on normal blood vessels. Nevertheless, it has been detected by immunohistochemistry in the prostate, kidney, liver, intestine, and colon, as well as on astrocytes of the brain (30,44,45). Discrepancies exist between these studies, however, and interpretation of the data is complicated by the existence of splice variants (12,13), localization of protein on the cell surface (apical *versus* basal), process of tissue collection, method of fixation, and the antibodies used to detect PSMA. Recognition of PSMA by our CAR T cells is mediated through the well-characterized scFv, J591. Encouragingly, imaging studies performed with radiolabeled J591 did not show accumulation of the mAb in either the kidneys or the small intestine (46). Furthermore, a phase 1 clinical trial with the J591 mAb demonstrated positive localization of the antibody to tumors with $PSMA^+$ vasculature (47). Overall, this evidence suggests that J591-based CAR T cells will have a favorable safety profile in patients. Still, given the catastrophic potential of eliciting "on-target/off-tumor" toxicity, we propose that the creation of split-signaling CAR T cells could augment the safety of our current anti-PSMA T cells. Using this system, T cells could be engineered to express two CARs, one providing signal 1 (CD3ζ) and the second providing signal 2 (i.e. CD28 and/or 4-1BB), such that each recognizes a unique tumor vascular antigen. The feasibility of this approach was previously demonstrated by Lanitis and colleagues (22), who showed that split-signaling CAR T cells are only fully activated when both CARs are engaged. Additional tumor endothelial targets have been identified in ovarian cancer (4, 48) as well as other tumors (49), enabling such combinatorial designs.

PSMA expression has been reported on the vasculature of nearly every solid tumor type examined (Supplementary Fig. 3A). This suggests that its presence may be critical to the formation of new blood vessels within the tumor. Here we found that 85% of women with ovarian cancer expressed PSMA on their tumor vasculature but only 40–60% of the $CD31^+$ tumor endothelial cells were $PSMA^+$. The presence of PSMA on the tumor vasculature may be partially explained by the increased metabolic needs of the activated tumor endothelium and may reflect a requirement for increased folate uptake. Functionally, PSMA hydrolyzes the gamma-glutamyl tail of folate polyglutamates, allowing cells to take up the resulting folates readily. At physiological folate concentrations the overexpression of PSMA was shown to confer growth advantage to tumor cells and enhance their invasive activity, potentially suggesting a similar role for the protein on the tumor endothelium (15). In addition, a direct role for PSMA in angiogenesis has been described, as the process was severely impaired in PSMA-null mice. In these mice the enzymatic activity of PSMA was required for endothelial cell invasion *in vitro* through regulation of integrin signaling, potentially explaining this phenotype (16). Therefore, we have hypothesized that PSMA-expressing endothelial cells are critical for neovascular formation, and that their persistent immune-mediated elimination by CAR T cells both disrupts the existing vasculature and prevents the formation of new blood vessels. These inquiries provide further rationale for

the development of anti-PSMA CAR T-cell therapy targeting the tumor vasculature, and are actively being addressed within our lab.

In our $MS1^{PSMA}/ID8^{VEGF}$ tumor model, we showed that adoptively transferred P28BBζ CAR T cells were able to persistently suppress nearly the entire PSMA-expressing fraction of the tumor endothelium. Their elimination, however, did not result in complete tumor regression. This could be because only a fraction of the tumor endothelial cells expressed PSMA within this model, similar to the human tumor specimens we analyzed. One method to overcome this obstacle would be to combine our anti-PSMA CAR T cells with additional treatment modalities. Conventional VDAs have been combined with both radiotherapy and chemotherapy for improved tumor control (50), suggesting that a similar approach could also augment the efficacy T cell-mediated vascular disruption. In addition, VDAs have also been successfully administered with anti-angiogenic agents as a means to target the existing tumor blood vessels, as well as impair the growth of new vessels (51). This has already been demonstrated using 1^{st} generation CAR T cells directed against the VEGF receptors, and these T cells were found to synergize with anti-angiogenic therapy (11). Another approach to increase the efficacy of our anti-PSMA CAR T cells would be to combine them with CAR T cells or TCR-engineered T cells that recognize a second tumor endothelial antigen or the tumor itself. Steven Rosenberg and colleagues have illustrated this approach by showing that B16 tumors could be successfully eradicated in mice when anti-VEGFR-2 CAR T cells were combined with tumor-targeting T cells, but not when the mice were treated with the anti-vascular CAR T cells alone (52). Building on this observation, we also posit that patients whose tumor expresses PSMA on both the endothelium and tumor, as was observed here for one subject with ovarian cancer and has been noted in a number of cancers (30), may respond more successfully to treatment with our anti-PSMA T cells. We continue to pursue the answer to this question within our lab.

In conclusion, we have demonstrated that 3^{rd} generation CAR T cells can target and eliminate PSMA-expressing endothelial cells of the tumor vasculature both *in vitro* and *in vivo*, and that elimination of these cells can result in tumor regression. We propose that split-signaling may enhance their safety profile, and that, in combination with other treatments such as chemotherapy, radiation, and/or tumor cell-targeting T cells, they will provide important clinical benefit to patients.

Supplementary Material

Refer to Web version on PubMed Central for supplementary material.

Acknowledgments

We would like to thank Michel Sadelain (Memorial Sloan Kettering Cancer Center) for generously providing the J591 scFv, Carl H. June (University of Pennsylvania) for generously providing his lentiviral expression cassettes, and Neil H. Bander (Cornell) for use of the humanized J591 antibody.

Grant Support
This project was supported by NIH transformative R01CA156695 and ERC Advanced grant 1400206AdG–322875 (GC), NCI training grant R25CA101871 (SPS), NCI training grant T32CA009140 (GTM), NCI SPORE in Ovarian Cancer P50CA083638-14 (GC, CL), the Ovarian Cancer Research Fund (GC), the Leenaards Foundation (GC), grant IRG-78-002-35 from the American Cancer Society, and the Sandy Rollman Ovarian Cancer Foundation (CL).

Citations

1. Bergers G, Benjamin LE. Tumorigenesis and the angiogenic switch. Nat Rev Cancer. 2003; 3:401–10. [PubMed: 12778130]
2. Neiva KG, Warner KA, Campos MS, Zhang Z, Moren J, Danciu TE, et al. Endothelial cell-derived interleukin-6 regulates tumor growth. BMC Cancer. 2014; 14:99. [PubMed: 24533454]
3. Lu J, Ye X, Fan F, Xia L, Bhattacharya R, Bellister S, et al. Endothelial cells promote the colorectal cancer stem cell phenotype through a soluble form of Jagged-1. Cancer Cell. 2013; 23:171–85. [PubMed: 23375636]
4. Buckanovich RJ, Facciabene A, Kim S, Benencia F, Sasaroli D, Balint K, et al. Endothelin B receptor mediates the endothelial barrier to T cell homing to tumors and disables immune therapy. Nat Med. 2008; 14:28–36. [PubMed: 18157142]
5. Motz GT, Santoro SP, Wang LP, Garrabrant T, Lastra RR, Hagemann IS, et al. Tumor endothelium FasL establishes a selective immune barrier promoting tolerance in tumors. Nat Med. 2014; 20:607–15. [PubMed: 24793239]
6. Dotti G, Gottschalk S, Savoldo B, Brenner MK. Design and development of therapies using chimeric antigen receptor-expressing T cells. Immunol Rev. 2014; 257:107–26. [PubMed: 24329793]
7. Smith NR, Baker D, James NH, Ratcliffe K, Jenkins M, Ashton SE, et al. Vascular endothelial growth factor receptors VEGFR-2 and VEGFR-3 are localized primarily to the vasculature in human primary solid cancers. Clin Cancer Res. 2010; 16:3548–61. [PubMed: 20606037]
8. Chinnasamy D, Yu Z, Theoret MR, Zhao Y, Shrimali RK, Morgan RA, et al. Gene therapy using genetically modified lymphocytes targeting VEGFR-2 inhibits the growth of vascularized syngenic tumors in mice. J Clin Invest. 2010; 120:3953–68. [PubMed: 20978347]
9. Niederman TM, Ghogawala Z, Carter BS, Tompkins HS, Russell MM, Mulligan RC. Antitumor activity of cytotoxic T lymphocytes engineered to target vascular endothelial growth factor receptors. Proc Natl Acad Sci U S A. 2002; 99:7009–14. [PubMed: 11997459]
10. Chang SS, O'Keefe DS, Bacich DJ, Reuter VE, Heston WD, Gaudin PB. Prostate-specific membrane antigen is produced in tumor-associated neovasculature. Clin Cancer Res. 1999; 5:2674–81. [PubMed: 10537328]
11. Chang SS, Reuter VE, Heston WD, Bander NH, Grauer LS, Gaudin PB. Five different anti-prostate-specific membrane antigen (PSMA) antibodies confirm PSMA expression in tumor-associated neovasculature. Cancer Res. 1999; 59:3192–8. [PubMed: 10397265]
12. Cao KY, Mao XP, Wang DH, Xu L, Yuan GQ, Dai SQ, et al. High expression of PSM-E correlated with tumor grade in prostate cancer: a new alternatively spliced variant of prostate-specific membrane antigen. The Prostate. 2007; 67:1791–800. [PubMed: 17929272]
13. Schmittgen TD, Teske S, Vessella RL, True LD, Zakrajsek BA. Expression of prostate specific membrane antigen and three alternatively spliced variants of PSMA in prostate cancer patients. Int J Cancer. 2003; 107:323–9. [PubMed: 12949815]
14. Su SL, Huang IP, Fair WR, Powell CT, Heston WD. Alternatively spliced variants of prostate-specific membrane antigen RNA: ratio of expression as a potential measurement of progression. Cancer Res. 1995; 55:1441–3. [PubMed: 7882349]
15. Yao V, Berkman CE, Choi JK, O'Keefe DS, Bacich DJ. Expression of prostate-specific membrane antigen (PSMA), increases cell folate uptake and proliferation and suggests a novel role for PSMA in the uptake of the non-polyglutamated folate, folic acid. The Prostate. 2010; 70:305–16. [PubMed: 19830782]
16. Conway RE, Petrovic N, Li Z, Heston W, Wu D, Shapiro LH. Prostate-specific membrane antigen regulates angiogenesis by modulating integrin signal transduction. Mol Cell Biol. 2006; 26:5310–24. [PubMed: 16809768]
17. Colombatti M, Grasso S, Porzia A, Fracasso G, Scupoli MT, Cingarlini S, et al. The prostate specific membrane antigen regulates the expression of IL-6 and CCL5 in prostate tumour cells by activating the MAPK pathways. PloS One. 2009; 4:e4608. [PubMed: 19242540]

18. Zhong XS, Matsushita M, Plotkin J, Riviere I, Sadelain M. Chimeric antigen receptors combining 4-1BB and CD28 signaling domains augment PI3kinase/AKT/Bcl-XL activation and CD8+ T cell-mediated tumor eradication. Mol Ther. 2010; 18:413–20. [PubMed: 19773745]
19. Song DG, Ye Q, Carpenito C, Poussin M, Wang LP, Ji C, et al. In vivo persistence, tumor localization, and antitumor activity of CAR-engineered T cells is enhanced by costimulatory signaling through CD137 (4-1BB). Cancer Res. 2011; 71:4617–27. [PubMed: 21546571]
20. Carpenito C, Milone MC, Hassan R, Simonet JC, Lakhal M, Suhoski MM, et al. Control of large, established tumor xenografts with genetically retargeted human T cells containing CD28 and CD137 domains. Proc Natl Acad Sci U S A. 2009; 106:3360–5. [PubMed: 19211796]
21. Dull T, Zufferey R, Kelly M, Mandel RJ, Nguyen M, Trono D, et al. A third-generation lentivirus vector with a conditional packaging system. J Virol. 1998; 72:8463–71. [PubMed: 9765382]
22. Lanitis E, Poussin M, Hagemann IS, Coukos G, Sandaltzopoulos R, Scholler N, et al. Redirected antitumor activity of primary human lymphocytes transduced with a fully human anti-mesothelin chimeric receptor. Mol Ther. 2012; 20:633–43. [PubMed: 22127019]
23. Garlanda C, Parravicini C, Sironi M, De Rossi M, Wainstok de Calmanovici R, Carozzi F, et al. Progressive growth in immunodeficient mice and host cell recruitment by mouse endothelial cells transformed by polyoma middle-sized T antigen: implications for the pathogenesis of opportunistic vascular tumors. Proc Natl Acad Sci U S A. 1994; 91:7291–5. [PubMed: 8041783]
24. Ades EW, Candal FJ, Swerlick RA, George VG, Summers S, Bosse DC, et al. HMEC-1: establishment of an immortalized human microvascular endothelial cell line. J Invest Dermatol. 1992; 99:683–90. [PubMed: 1361507]
25. Liu H, Moy P, Kim S, Xia Y, Rajasekaran A, Navarro V, et al. Monoclonal antibodies to the extracellular domain of prostate-specific membrane antigen also react with tumor vascular endothelium. Cancer Res. 1997; 57:3629–34. [PubMed: 9288760]
26. Denmeade SR, Mhaka AM, Rosen DM, Brennen WN, Dalrymple S, Dach I, et al. Engineering a prostate-specific membrane antigen-activated tumor endothelial cell prodrug for cancer therapy. Sci Transl Med. 2012; 4:140ra86.
27. Kalli KR, Oberg AL, Keeney GL, Christianson TJ, Low PS, Knutson KL, et al. Folate receptor alpha as a tumor target in epithelial ovarian cancer. Gynecol Oncol. 2008; 108:619–26. [PubMed: 18222534]
28. Markert S, Lassmann S, Gabriel B, Klar M, Werner M, Gitsch G, et al. Alpha-folate receptor expression in epithelial ovarian carcinoma and non-neoplastic ovarian tissue. Anticancer Res. 2008; 28:3567–72. [PubMed: 19189636]
29. O'Shannessy DJ, Somers EB, Smale R, Fu YS. Expression of folate receptor-alpha (FRA) in gynecologic malignancies and its relationship to the tumor type. Int J Gynecol Pathol. 2013; 32:258–68. [PubMed: 23518909]
30. Mhawech-Fauceglia P, Zhang S, Terracciano L, Sauter G, Chadhuri A, Herrmann FR, et al. Prostate-specific membrane antigen (PSMA) protein expression in normal and neoplastic tissues and its sensitivity and specificity in prostate adenocarcinoma: an immunohistochemical study using mutiple tumour tissue microarray technique. Histopathology. 2007; 50:472–83. [PubMed: 17448023]
31. Arbiser JL, Moses MA, Fernandez CA, Ghiso N, Cao Y, Klauber N, et al. Oncogenic H-ras stimulates tumor angiogenesis by two distinct pathways. Proc Natl Acad Sci U S A. 1997; 94:861–6. [PubMed: 9023347]
32. Thorpe PE. Vascular targeting agents as cancer therapeutics. Clin Cancer Res. 2004; 10:415–27. [PubMed: 14760060]
33. Lutz AM, Bachawal SV, Drescher CW, Pysz MA, Willmann JK, Gambhir SS. Ultrasound molecular imaging in a human CD276 expression-modulated murine ovarian cancer model. Clin Cancer Res. 2014; 20:1313–22. [PubMed: 24389327]
34. Chacko AM, Li C, Nayak M, Mikitsh JL, Hu J, Hou C, et al. Development of 124I immuno-PET targeting tumor vascular TEM1/endosialin. J Nuclear Med. 2014; 55:500–7.
35. Li C, Chacko AM, Hu J, Hasegawa K, Swails J, Grasso L, et al. Antibody-based tumor vascular theranostics targeting endosialin/TEM1 in a new mouse tumor vascular model. Cancer Biol Ther. 2014; 15:443–51. [PubMed: 24553243]

36. Zhang L, Yang N, Garcia JR, Mohamed A, Benencia F, Rubin SC, et al. Generation of a syngeneic mouse model to study the effects of vascular endothelial growth factor in ovarian carcinoma. Am J Pathol. 2002; 161:2295–309. [PubMed: 12466143]
37. Moreno Garcia V, Basu B, Molife LR, Kaye SB. Combining antiangiogenics to overcome resistance: rationale and clinical experience. Clin Cancer Res. 2012; 18:3750–61. [PubMed: 22547772]
38. Kalos M, Levine BL, Porter DL, Katz S, Grupp SA, Bagg A, et al. T cells with chimeric antigen receptors have potent antitumor effects and can establish memory in patients with advanced leukemia. Sci Transl Med. 2011; 3:95ra73.
39. Brentjens RJ, Davila ML, Riviere I, Park J, Wang X, Cowell LG, et al. CD19-targeted T cells rapidly induce molecular remissions in adults with chemotherapy-refractory acute lymphoblastic leukemia. Sci Transl Med. 2013; 5:177ra38.
40. Porter DL, Levine BL, Kalos M, Bagg A, June CH. Chimeric antigen receptor-modified T cells in chronic lymphoid leukemia. N Engl J Med. 2011; 365:725–33. [PubMed: 21830940]
41. Louis CU, Savoldo B, Dotti G, Pule M, Yvon E, Myers GD, et al. Antitumor activity and long-term fate of chimeric antigen receptor-positive T cells in patients with neuroblastoma. Blood. 2011; 118:6050–6. [PubMed: 21984804]
42. Beatty GL, Haas AR, Maus MV, Torigian DA, Soulen MC, Plesa G, et al. Mesothelin-specific Chimeric Antigen Receptor mRNA-Engineered T cells Induce Anti-Tumor Activity in Solid Malignancies. Cancer Immunol Res. 2014; 2:112–20. [PubMed: 24579088]
43. Gilham DE, Debets R, Pule M, Hawkins RE, Abken H. CAR-T cells and solid tumors: tuning T cells to challenge an inveterate foe. Trends Mol Med. 2012; 18:377–84. [PubMed: 22613370]
44. Kinoshita Y, Kuratsukuri K, Landas S, Imaida K, Rovito PM Jr, Wang CY, et al. Expression of prostate-specific membrane antigen in normal and malignant human tissues. World J Surgery. 2006; 30:628–36.
45. Silver DA, Pellicer I, Fair WR, Heston WD, Cordon-Cardo C. Prostate-specific membrane antigen expression in normal and malignant human tissues. Clin Cancer Res. 1997; 3:81–5. [PubMed: 9815541]
46. Bander NH, Trabulsi EJ, Kostakoglu L, Yao D, Vallabhajosula S, Smith-Jones P, et al. Targeting metastatic prostate cancer with radiolabeled monoclonal antibody J591 to the extracellular domain of prostate specific membrane antigen. J Urology. 2003; 170:1717–21.
47. Milowsky MI, Nanus DM, Kostakoglu L, Sheehan CE, Vallabhajosula S, Goldsmith SJ, et al. Vascular targeted therapy with anti-prostate-specific membrane antigen monoclonal antibody J591 in advanced solid tumors. J Clin Oncol. 2007; 25:540–7. [PubMed: 17290063]
48. Sasaroli D, Gimotty PA, Pathak HB, Hammond R, Kougioumtzidou E, Katsaros D, et al. Novel surface targets and serum biomarkers from the ovarian cancer vasculature. Cancer Biol Ther. 2011; 12:169–80. [PubMed: 21617380]
49. St Croix B, Rago C, Velculescu V, Traverso G, Romans KE, Montgomery E, et al. Genes expressed in human tumor endothelium. Science. 2000; 289:1197–202. [PubMed: 10947988]
50. Horsman MR, Siemann DW. Pathophysiologic effects of vascular-targeting agents and the implications for combination with conventional therapies. Cancer Res. 2006; 66:11520–39. [PubMed: 17178843]
51. Siemann DW, Shi W. Dual targeting of tumor vasculature: combining Avastin and vascular disrupting agents (CA4P or OXi4503). Anticancer Res. 2008; 28:2027–31. [PubMed: 18751370]
52. Chinnasamy D, Tran E, Yu Z, Morgan RA, Restifo NP, Rosenberg SA. Simultaneous targeting of tumor antigens and the tumor vasculature using T lymphocyte transfer synergize to induce regression of established tumors in mice. Cancer Res. 2013; 73:3371–80. [PubMed: 23633494]

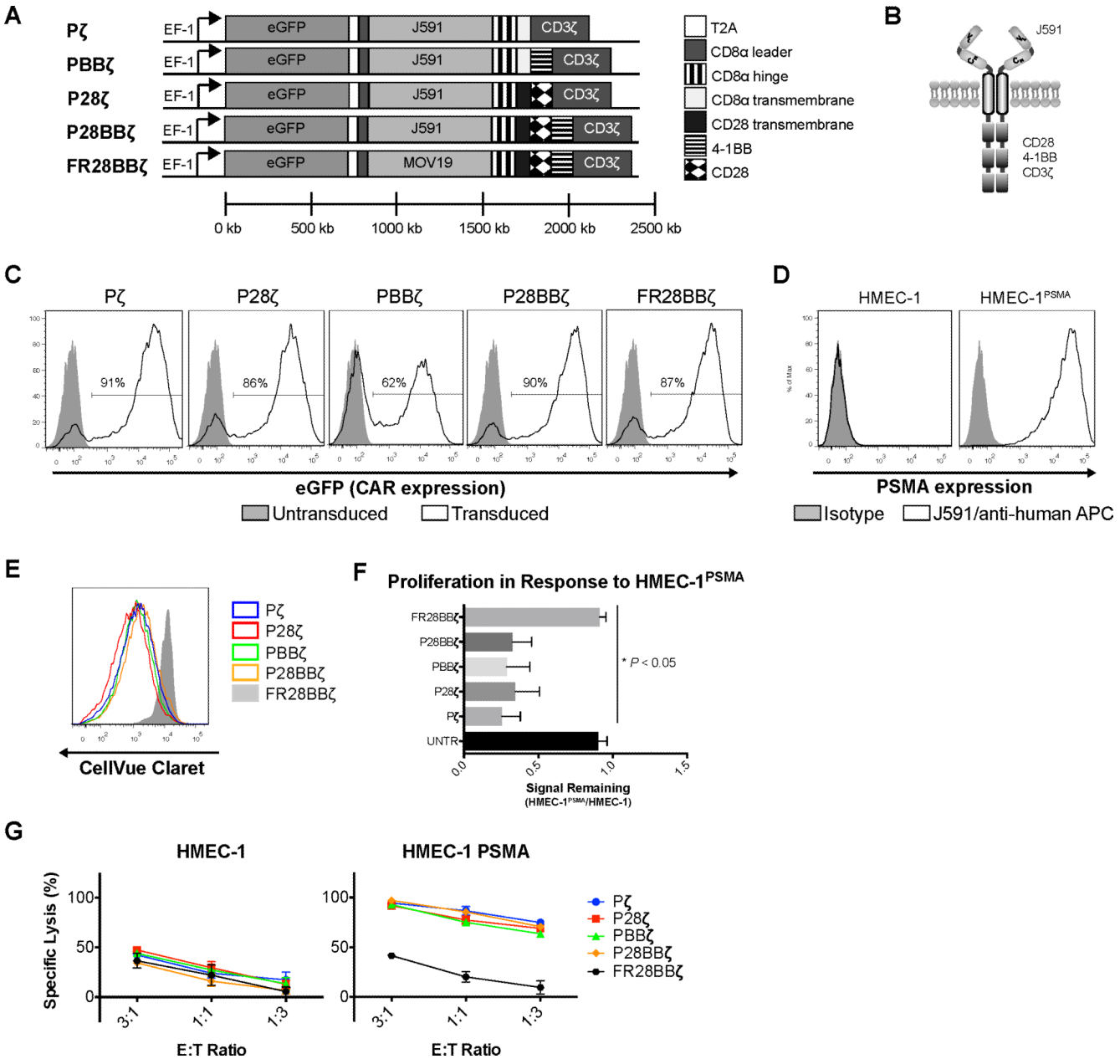

Figure 1. Design and characterization of an anti-vascular CAR

(A) Lentiviral cassette design for the J591-based CAR constructs: Pζ, P28ζ, PBBζ, P28BBζ and the FR28BBζ specificity control. (B) Schematic representation of the P28BBζ CAR. (C) Representative transduction efficiencies, as measured by eGFP reporter, for the CAR constructs in primary human T cells. Closed histograms depict untransduced cells; open histograms depict transduced T cells. (D) Human PSMA expression on the HMEC-1 and the engineered HMEC-1^{PSMA} endothelial cell lines. PSMA was detected by humanized J591 Ab (open histogram) and compared with human IgG control (closed histogram). (E) Overlay of histograms comparing the proliferative capacity of the T-cell groups 5 days after co-culture with HMEC-1^{PSMA}. (F) Quantitative comparison of proliferation between CAR constructs harboring different signaling domains. The geometric mean fluorescence intensity of

Cellvue® Claret staining was measured for the CAR-positive T cells after 5 days in co-culture with either HMEC-1 or HMEC-1^{PSMA} (E:T = 2:1). To normalize across multiple donors, the MFI of CellVue® staining on CAR^+ T cells after co-culture with HMEC-1^{PSMA} was divided by the MFI of the CAR^+ T cells after co-culture with the HMEC-1. *$P < 0.05$; data are means ±SEM from three independent donors. (G) Cytolytic activity of the various T cells after 18 h co-culture with HMEC-1 or HMEC-1^{PSMA}. Lysis was measured via luciferase assay (specific lysis = 100 – (luciferase signal treated/luciferase signal untreated × 100)). Data are means ±SD from triplicate cultures.

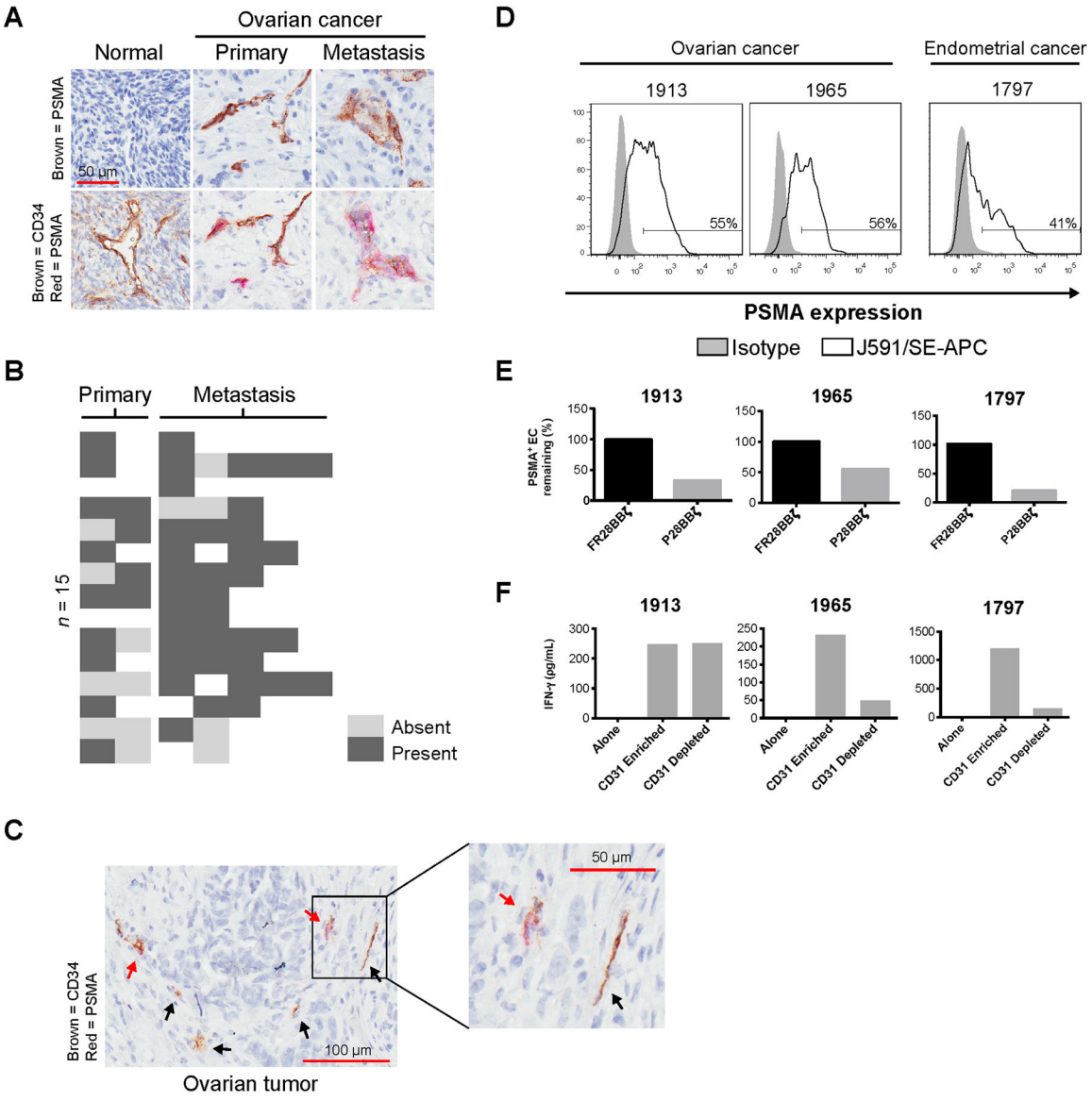

Figure 2. PSMA is expressed on the vasculature of primary and metastatic cancer.<
br>(A) Representative staining for PSMA (top row), as well as PSMA and the endothelial marker, CD34 (bottom row). Sequential sections were cut and stained for either PSMA alone, or PSMA with CD34. Images in each column depict the same region within the same core. Original magnification, 200×; scale bar, 50 μm. (B) A heat map showing the presence or absence of PSMA on the vasculature of tumors taken from subjects with resected ovarian cancer (*n* = 15). (C) Representative tumor core staining for both PSMA (red) and CD34 (brown). Black arrows indicate $CD34^+$ vessels that are negative for PSMA expression; red arrows indicate dual-positive ($CD34^+PSMA^+$) vessels. (D) Level of PSMA expression on tumor endothelial cells ($CD45^-CD31^+$) from three subjects with gynecologic cancer. Tumor endothelial cells were collected by CD45 depletion followed by CD31 enrichment. PSMA was detected by humanized J591 Ab (open histogram) and compared with human IgG control (closed histogram). (E) The percentage of PSMA-positive $CD45^-CD31^+$ endothelial

cells remaining after overnight co-culture with CAR T cells (E:T = 1:1). Percentage = treated/untreated × 100. (F) IFNγ production by P28BBζ T cells after co-culture with CD31 enriched or depleted targets (E:T = 1:1). Culture supernatants were collected at 18 h and IFNγ was measured by ELISA.

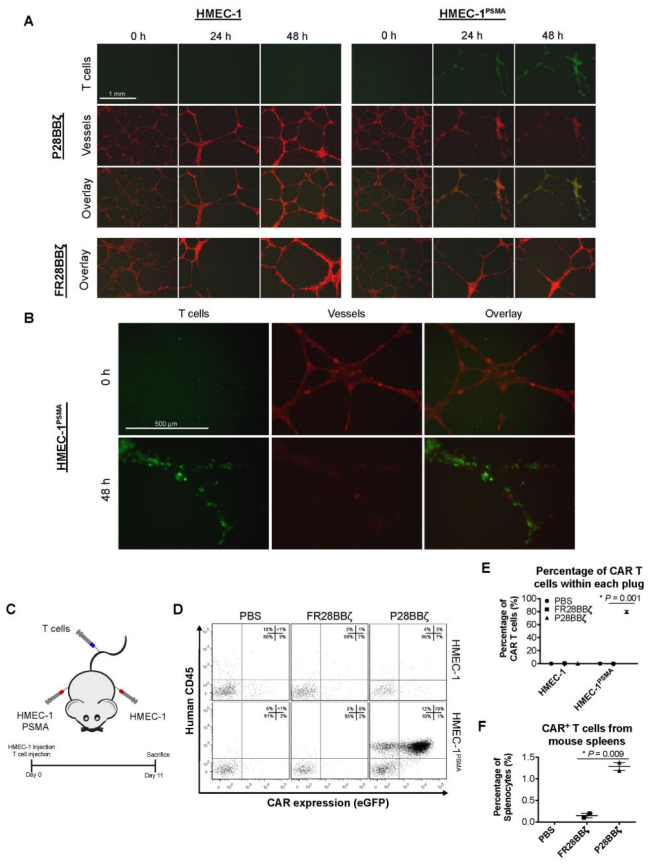

Figure 3. P28BBζ CAR T cells target human tumor vasculature expressing PSMA.
(A) Antigen-specific destruction of HMEC-1^{PSMA} microvessels after 48 h co-culture with P28BBζ T cells. HMEC-1 or HMEC-1^{PSMA} endothelial cells (RFP, red) were seeded atop a Matrigel basement membrane and allowed to form microvessels for 8 h prior to co-culture with CAR-bearing T cells (eGFP, green) (E:T = 3:1). Images were taken at 0, 24, and 48 h. Original magnification, 40×; scale bar, 1 mm. (B) Immunofluorescence images of the HMEC-1^{PSMA} endothelial cells at initiation (0 h) and termination (48 h) of co-culture with the P28BBζ T cells. Original magnification, 100×; scale bar, 500 μm. (C) Experimental design for the HMEC-1 pilot study. Mice were injected s.c. on each flank with 1.0×10^6 HMEC-1 (left flank) and 1.0×10^6 HMEC-1^{PSMA} (right flank) endothelial cells. T cells were administered concurrently via i.v. injection. Treated mice received 5.0×10^6 CAR-positive T cells. (D) Representative dot plots from treated or control mice showing human CD45 and CAR (eGFP) expression. Matrigel plugs were retrieved upon sacrifice (11 d) and were digested to yield a single-cell suspension. Cells were subsequently stained for human CD45 and analyzed for eGFP expression using a flow cytometer. (E) CAR T cells as a percentage of the cells isolated from the Matrigel plugs. *P = 0.001, as determined by two-tailed Student's t test. n = 2 mice in the FR28BBζ and P28BBζ; n = 1 mouse in the untreated (PBS) group. Data are means ±SEM. (F) CAR T cells as a percentage of total splenocytes. Spleens were isolated from mice upon sacrifice, mechanically disrupted, and analyzed for the presence of CAR T cells (eGFP). *P = 0.009, as determined by two-tailed Student's t

test. $n = 2$ mice in the FR28BBζ and P28BBζ; $n = 1$ mouse in the untreated (PBS) group. Data are means ±SEM.

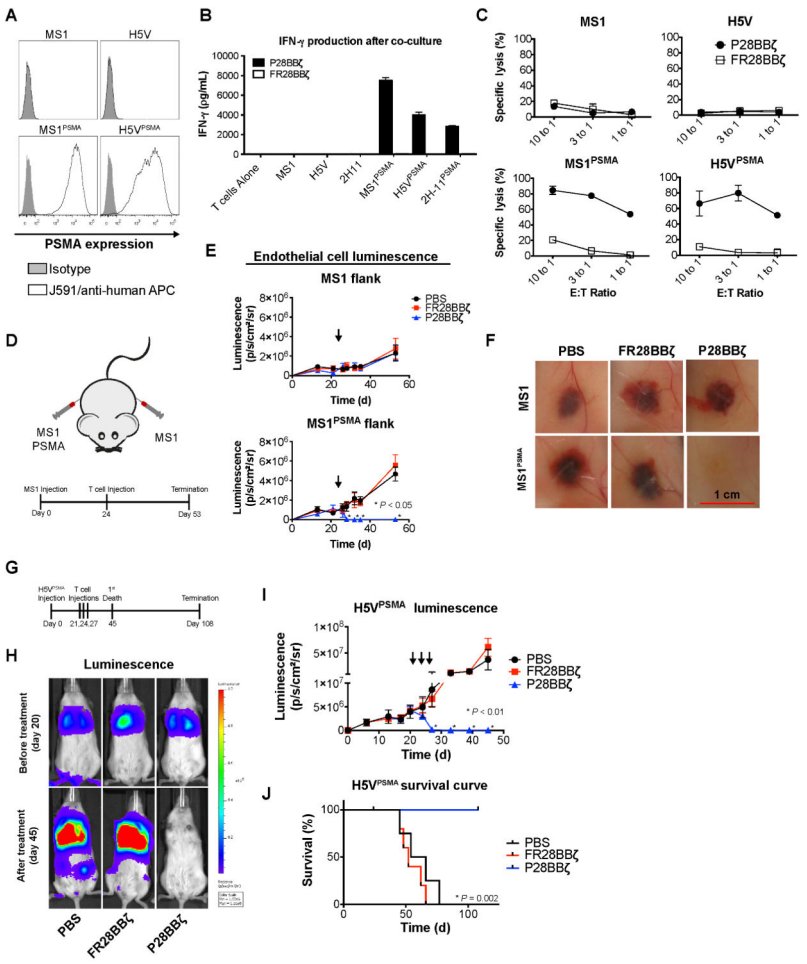

Figure 4. P28BBζ CAR T cells eliminate PSMA$^+$ vascular neoplasms.<

br>(A) Human PSMA expression on native (top row) and engineered (bottom row) murine endothelial cell lines. PSMA was detected by humanized J591 Ab (open histogram) and compared with human IgG control (closed histogram). (B) IFNγ production by P28BBζ T cells after co-culture with endothelial targets (E:T = 3:1). Culture supernatants were collected at 18 h and IFNγ was measured by ELISA. Representative donor shown; data are means ±SD of triplicate cultures. (C) Cytolytic activity of P28BBζ T cells after 18 h co-culture with endothelial cell targets. Cell lysis measured by chromium release. Representative donor shown; data are means ±SD of triplicate cultures. (D) Tumor injection schematic and experimental design for the MS1 hemangioma study. Mice were injected s.c. on each flank with 1.0×10^7 MS1 (left flank) and 1.0×10^7 MS1^{PSMA} (right flank) endothelial cells. Hemangiomas were allowed to develop for 24 days prior to i.v. injection of T cells. (E) Tumor progression, as measured by luciferase luminescence, in mice receiving PBS, FR28BBζ, or P28BBζ T cells. Mice were given a single injection of 5.0×10^6 CAR-positive T cells (arrows) 24 days after inoculation with tumor. $n = 5$ mice per group; data are means ±SEM. $^*P < 0.05$, as determined by two-tailed Student's t test, for the P28BBζ treated group when compared to the FR28BBζ control group at the indicated time points. (F) Representative hemangiomas at the time of sacrifice (day 53). (G) Experimental design for

the H5V hemangiosarcoma tumor study. Mice were injected i.v. with 5.0×10^5 $H5V^{PSMA}$ endothelial cells. Lung tumors were allowed to engraft for 3 weeks prior to administration of T cells. (H) Tumor progression, as measured by luciferase luminescence, in mice receiving PBS, FR28BBζ, or P28BBζ T cells. Mice were given three injections of 5.0×10^6 CAR-positive T cells beginning 21 days after tumor inoculation (arrows). $n = 5$ mice per group; data are means ±SEM. $^*P < 0.05$, as determined by two-tailed Student's t test, for the P28BBζ treated group when compared to the FR28BBζ control group at the indicated time points. (I) Survival curve for mice with $H5V^{PSMA}$ tumors. P28BBζ treated mice were sacrificed on day 108. $P = 0.002$, as determined by log-ranked (Mantel-Cox) test. $n = 5$ mice per group. (J) Tumor luminescence in representative mice before (day 20) and after T cell treatment (day 45).

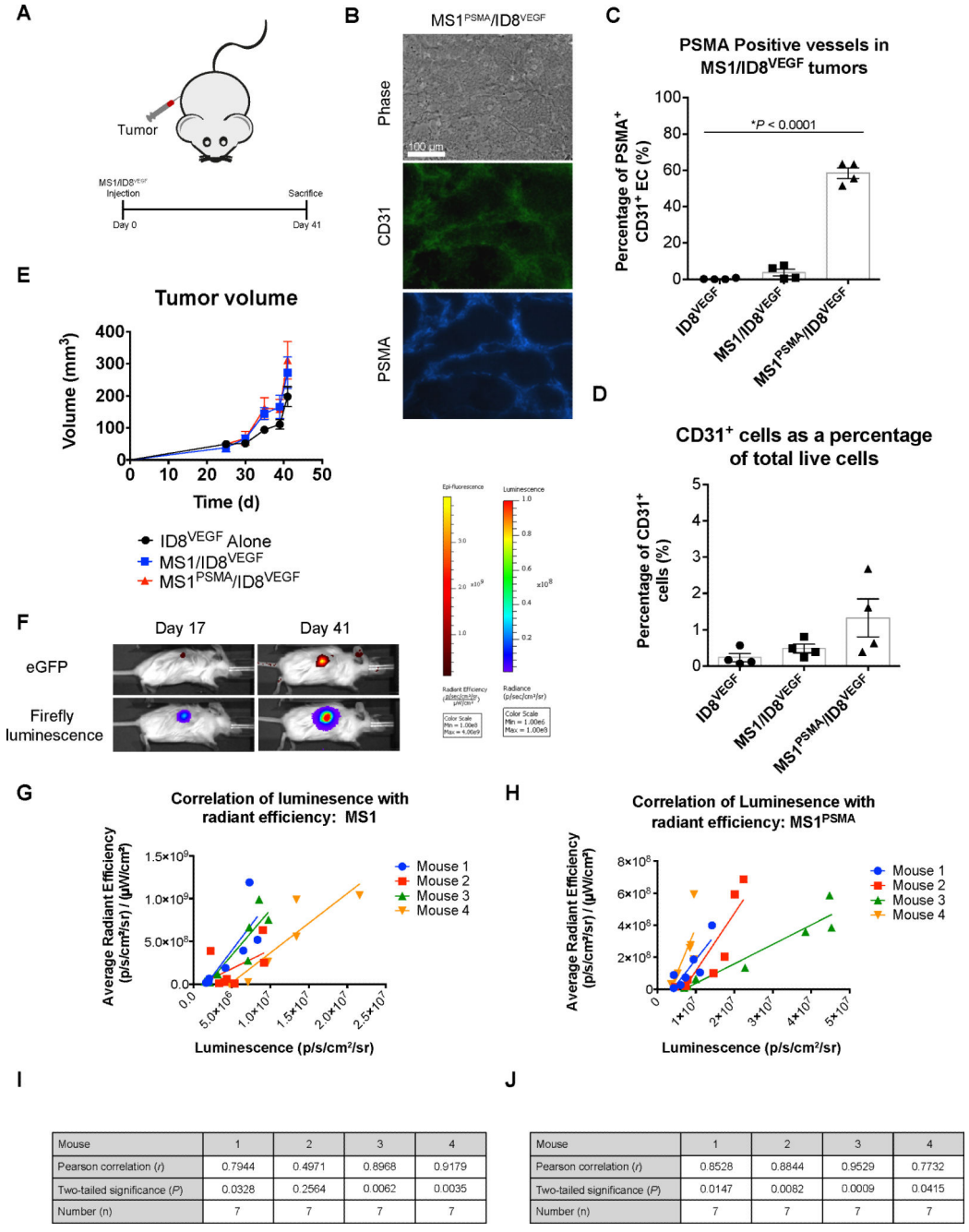

Mouse	1	2	3	4
Pearson correlation (*r*)	0.7944	0.4971	0.8968	0.9179
Two-tailed significance (*P*)	0.0328	0.2564	0.0062	0.0035
Number (n)	7	7	7	7

Mouse	1	2	3	4
Pearson correlation (*r*)	0.8528	0.8844	0.9529	0.7732
Two-tailed significance (*P*)	0.0147	0.0082	0.0009	0.0415
Number (n)	7	7	7	7

Figure 5. The MS1/ID8^{VEGF} tumor model closely mimics normal tumor physiology.< br>(A) Tumor injection schematic and experimental design for the MS1/ID8^{VEGF} characterization study. Mice were given a single s.c. injection of 1.0×10^6 ID8^{VEGF} tumor cells either alone or with 1.5×10^7 MS1 or 1.5×10^7 MS1^{PSMA} endothelial cells and monitored for 41 days. (B) Representative staining for CD31 (green) and PSMA (blue) from an MS1^{PSMA}/ID8^{VEGF} tumor (d 41). Original magnification, 200×; scale bar, 100 μm. (C) The percentage of MS1^{PSMA}-derived endothelial cells (CD31$^+$) in ID8 tumors at time of sacrifice. PSMA was detected by humanized J591 Ab. *$P < 0.0001$, as determined by two-tailed Student's t test. $n = 4$ mice per group; data are means ±SEM. (D) The portion of

$CD31^+$ endothelial cells present in tumor digests reported as a percentage of the total number of live cells collected. $n = 4$ mice per group; data are means ±SEM. (E) Tumor progression in mice harboring $ID8^{VEGF}$, $MS1/ID8^{VEGF}$, or $MS1^{PSMA}/ID8^{VEGF}$ tumors. Tumor volumes were calculated via caliper measurement. $n = 4$ mice per group; data are means ±SEM. (F) Representative images taken from the same mouse on day 17 and 41 showing eGFP radiance and firefly luminescence. (G,H) Correlation of endothelial cell signal (firefly luciferase, luminescence) with tumor signal (eGFP, radiant efficiency). Linear regression analysis was performed and the slope of best fit is shown (solid lines) for individual mice with either $MS1/ID8^{VEGF}$ (f) or $MS1^{PSMA}/ID8^{VEGF}$ (g) tumors. (I,J) Statistical analysis describing the correlation of luminescence and radiant efficiency in mice with $MS1/ID8^{VEGF}$ (h) and $MS1^{PSMA}/ID8^{VEGF}$ (i) tumors. Measurements were made 17–41 days after tumor inoculation. Luciferase and radiant efficiency measurements were plotted against one another ($n = 7$) and Pearson correlation coefficients were calculated for each mouse (r). Statistical significance was evaluated by two-tailed test (P).

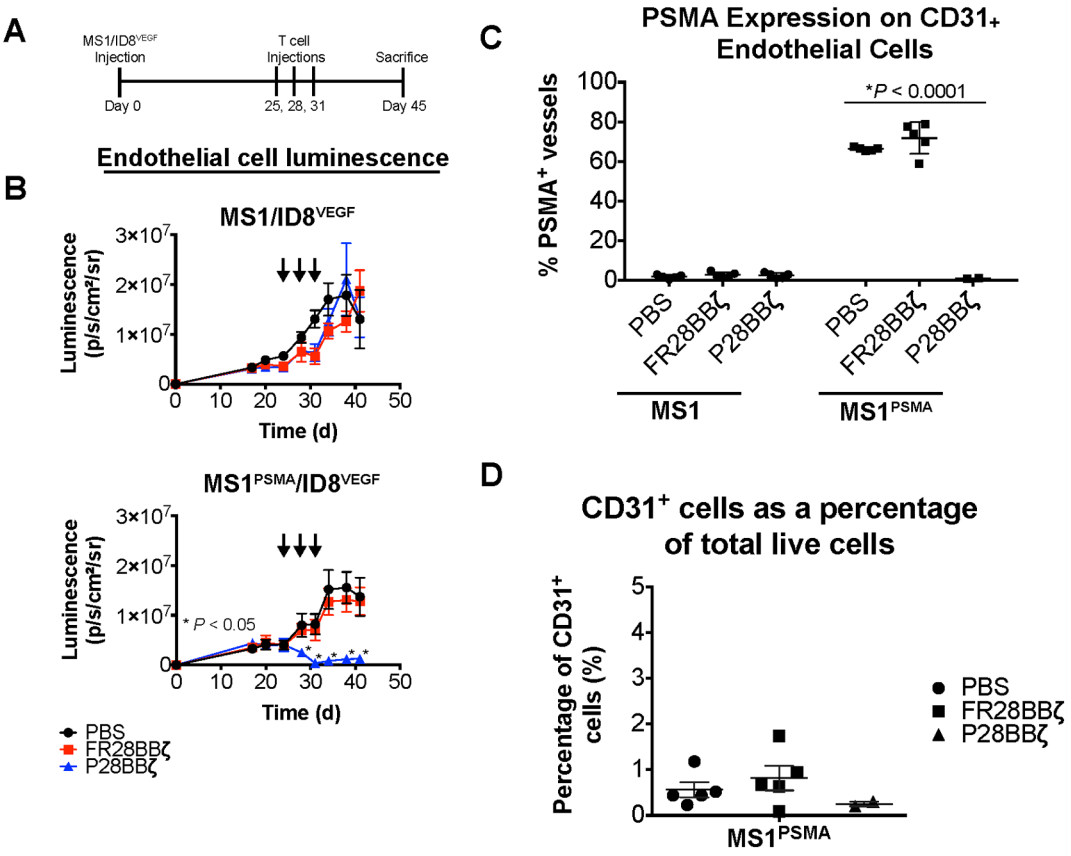

Figure 6. CAR T cells ablate PSMA$^+$ vasculature in solid tumors<

br>(A) Experimental design for the MS1/ID8^{VEGF} tumor study. 6.7×10^5 ID8^{VEGF} tumor cells were mixed with either 1.0×10^7 MS1 (left flank) or 1.0×10^7 MS1^{PSMA} (right flank) endothelial cells and injected s.c. on the opposite flanks of each mouse. Tumors were allowed to engraft for 25 days before treatment with CAR T cells. (B) The persistence of the MS1 and MS1^{PSMA} endothelial cells after treatment with PBS, FR28BBζ, or P28BBζ T cells. Mice were given three injections of 5.0×10^6 CAR-positive T cells beginning 25 days after tumor inoculation (arrows). The presence (or absence) of the MS1 and MS1^{PSMA} endothelial cells was monitored via luciferase luminescence. n = 5 mice per group; data are means ±SEM. *P < 0.05, as determined by two-tailed Student's t test, for the P28BBζ treated group when compared to the FR28BBζ control group at the indicated time points. (C) The percentage of PSMA positive tumor endothelial cells (CD45$^-$CD31$^+$) remaining after T cell administration to mice harboring MS1/ID8^{VEGF} and MS1^{PSMA}/ID8^{VEGF} tumors. PSMA was detected by humanized J591 Ab. *P < 0.0001, as determined by two-tailed Student's t test. n = 5 mice in the PBS and FR28BBζ groups; n = 2 mice in P28BBζ group. Data are means ±SEM. (D) The total percentage of tumor endothelial cells (CD45$^-$CD31$^+$) remaining in the MS1^{PSMA}/ID8^{VEGF} tumors after T cell administration. n = 5 mice in the PBS and FR28BBζ groups; n = 2 mice in P28BBζ group. Data are means ±SEM.

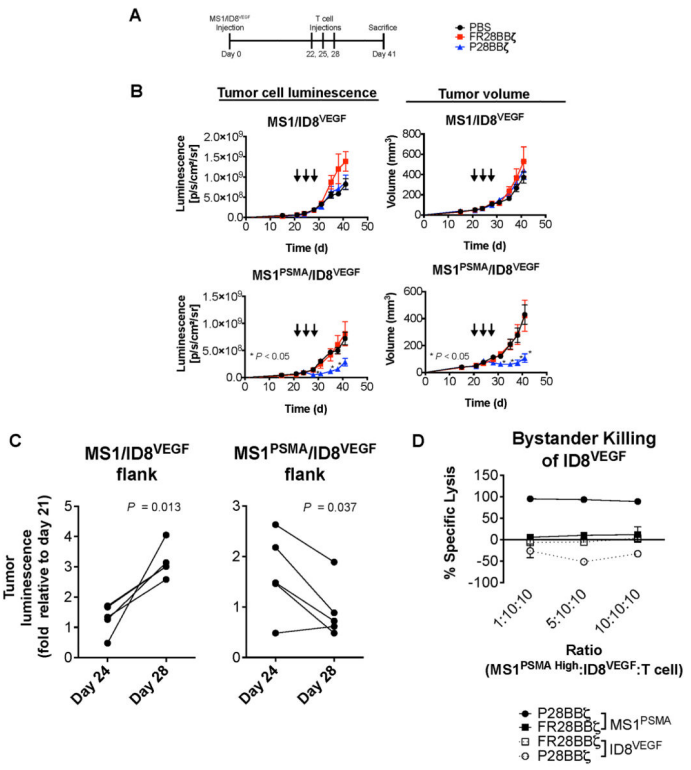

Figure 7. CAR T cells induce secondary loss of tumor cells and regression of solid tumors.
(A) Experimental design for the MS1/ID8^{VEGF} tumor study. 6.7×10^{5} ID8^{VEGF} tumor cells were mixed with either 1.0×10^{7} MS1 (left flank) or 1.0×10^{7} MS1^{PSMA} (right flank) endothelial cells and injected s.c. on opposite flanks of the same mice. Tumors were allowed to engraft for 22 days before T cell administration. (B) Tumor progression in mice receiving PBS, FR28BBζ, or P28BBζ T cells. Mice were given three injections of 5.0×10^{6} CAR-positive T cells beginning 22 days after tumor inoculation (arrows). The impact of T cell administration on the ID8^{VEGF} tumor cells was measured via luciferase luminescence (left column) and tumor volumes were calculated using caliper measurements (right column). *n* = 5 mice per group; data are means ±SEM. **P* < 0.05, as determined by two-tailed Student's t test, for the P28BBζ treated group when compared to the FR28BBζ control group at the indicated time points. (C) The fold-change in ID8^{VEGF} tumor cell luminescence from the MS1/ID8^{VEGF} and MS1^{PSMA}/ID8^{VEGF} tumors in mice receiving P28BBζ T cells. Luminescence measurements were normalized to those made prior to treatment (day 21). *P* values were determined by two-tailed Student's t test and reflect the statistical significance of changes between day 24 and day 28. *n* = 5. (D) P28BBζ T cells do not elicit bystander killing of ID8^{VEGF} when cultured in the presence of MS1^{PSMA}. MS1^{PSMA} cells were titrated into wells with ID8^{VEGF} tumor cells and T cells at the described ratios and were cultured for 18 h. Lysis was measured via luciferase assay (specific lysis = 100 – (luciferase signal treated/luciferase signal untreated × 100)). Data are means ±SD from triplicate cultures.